Article

Electromagnetic Metasurfaces: Insight into Evolution, Design and Applications

Khushboo Singh *[ID]**, Foez Ahmed** [ID] **and Karu Esselle** [ID]

School of Electrical and Data Engineering, University of Technology Sydney, Ultimo, NSW 2007, Australia
* Correspondence: khushboo.singh@uts.edu.au

Abstract: Metasurfaces have emerged as game-changing technology ranging from microwaves to optics. This article provides a roadmap to the evolution of electromagnetic metasurfaces with a focus on their synthesis techniques, materials used for their design and their recent and futuristic applications. A broad classification is provided, and the design principle is elaborated. The efficient and economical use of available computational resources is imperative to work with state-of-the-art metasurface systems. Hence, optimization becomes an integral part of metasurface design. Several optimization methodologies reported to date have been discussed. An extensive study on the current research database gathered a comprehensive understanding of meta-atom topologies and the preferred fabrication technologies. The study concludes with a critical analysis and highlights existing and future research challenges to be addressed.

Keywords: all-metal metasurface; all-dielectric metasurface; additive manufacturing; beam-steering; metamaterial; metasurface; meta-grating; metasurface antenna; optimization; 3D printing; phase-shifting-surface; phase-gradient surface; artificial surface; phase-correcting structure

1. Introduction

Metasurfaces are unequivocally excellent spatial processors with exotic surface waves that strongly enhance their electromagnetic (EM) wavefront control capabilities leading to fascinating physical effects and versatile applications. They are a promising candidate for real-world solutions. They have garnered significant interest and have seen tremendous advancement in recent years in almost all regimes of electromagnetic, acoustics and optics that have been elucidated in numerous review articles from different perspectives and areas of applications [1–7]. This review provides a blueprint for the evolution of metasurfaces to adapt to the growing need for arbitrary control of EM wave properties and overcome the limitations of naturally existing materials and metamaterials. The study focuses on the history and working principle of in-homogeneous metasurfaces in general and the electromagnetic applications of these metasurfaces in particular.

The discussion begins with the limitations of naturally existing materials and the advent of three-dimensional metamaterials to extend their capability for arbitrary EM wave manipulation. It is then emphasized how the evolution of two-dimensional metasurfaces addressed the bulky attribute of metamaterials and led to a new era of scientific innovations. The history, development and broad classification of metasurfaces and available synthesis methods constitute this study's body. An in-depth analysis for selecting materials in designing metasurfaces based on the application and several optimization approaches is also covered.

Physical systems that provides full control on properties of EM waves have a vital role in the current and upcoming generations of industrial revolution. Maxwell's equations suggest that the behaviour of an EM wave propagating in a medium is governed by the permittivity and the permeability of that medium. However, almost all naturally occurring materials have a very narrow range of permittivity variation and their permeability is very close to one, which renders a very limited control on the EM wave properties [8].

1.1. Metamaterials: Transcending Abilities of Natural Materials

The advent of metamaterials in late 90's led to an upsurge in the intriguing possibilities for tailoring the EM wave properties. Metamaterials are three dimensional (3D), artificially engineered EM media composed of sub-wavelength structures, often periodic and can exhibit any arbitrary values of permittivity and permeability [9]. The augmented parameter range bestows exceptional ability on metamaterials, which transcends all naturally occurring materials to control and transform EM waves. Due to their strong and exotic interaction with electric and/or magnetic fields, they demonstrate unique advantageous EM behavior, which actuated myriad fascinating applications in EM and optics engineering. Despite their diversified potentials and novel functionalities, metamaterials faced great challenges owing to their bulky profile, fabrication complexity, high insertion losses, mass production difficulty and high cost.

1.2. Metasurfaces: Dimensional Reduction of Metamaterials

The solution to the aforementioned problems of metamaterials was found in metasurfaces. Metasurfaces, which are often referred to as engineered EM surfaces, are free-standing artificial planar array of engineered identical or distinct sub-wavelength inclusions (with tailored response) arranged in a particular global sequence. In principle, a metasurface is a 2D analogue of a volumetric metamaterial. Unlike metamaterials, which rely on constitutive parameters in 3D space [9], metasurfaces manipulate the characteristics of propagating and evanescent waves by enforcing artificial boundary conditions on EM fields. Reduced physical profile due to surface confined wave-matter interactions made metasurfaces an attractive alternative to metamaterials. Tremendous research interest towards metasurfaces in many areas of applications is explained by their easy and cost-effective large-scale fabrication and the prospect of seamless device integration, as well as low insertion losses.

1.3. Metasurfaces: Past, Present and Future

Although, the thin composite interface discontinuities have been only recently referred to as metasurfaces, their concept and operating principle is not new. One of the earliest work was reported by Prof. H Lamb in 1896 [10], where he studied the reflection and transmission of electric wave (which he referred to as Hertzian wave) from a plane grating composed of equispaced metallic strips. The results and mathematical formula obtained in his work solved various problems in hydrodynamics, magnetic induction and acoustics. A few years later in 1902, Robert W. Wood observed unusual dark areas in the reflection spectrum of sub-wavelength metallic gratings, which he called as Wood's anomaly and it led to the discovery of Surface Plasmon Polariton (SPP). It provided a particular solution of surface waves at metal-dielectric interface [11]. Subsequently, another remarkable phenomenon was reported in [12] as Levi-Civita relation which shows that a dramatic change in EM boundary conditions occur at interface discontinuities of electrically small thickness.

In 1910, Marconi designed a polarization reflector using array of straight wires for telegraphy and telephony applications [13]. Metal wire meshes have a long history of being used as antenna reflectors and various screens. The optical properties of metallic mesh (wire grid) first observed in [14] in the year 1964 by studying the reflection and transmission properties of waves for normal and oblique incidence, are in principle the same phenomenon we observe in today's metasurfaces. A simple work reported in [15] investigated the solution of Maxwell's equation in hypothetical media having negative isotropic permittivity and permeability.

In 1998, the work reported by T.W. Ebbensen described some astounding optical transmission features with zero order transmission spectra through an array of sub-micron cylindrical cavities (holes) in the metal films [16]. The unconventional and innovative concept of perfect lensing by using negative refractive index materials proposed by J.B. Pendry in the year 2000 [17] was a major breakthrough in the advent of metamaterials that could efficiently reshape EM wavefronts. Since then, the metamaterials enjoyed the undivided attention of researchers for almost a decade before it succumbed to the grand

challenges of fabrication due to bulky profile and high insertion losses. A SPP based nanofabrication technique was proposed in 2004, to lithographically fabricate fine patterns beyond diffraction limit [18]. The phase delay concept of SPP was implemented in [19] to design a metallic beam deflector. This idea was further extended to derive and validate the generalized laws of reflection and refraction.

The anomalous reflection and refraction observed at an artificial interface consisting of an array of V-shaped metallic antenna was discussed in detail and the concept of judiciously and arbitrarily engineering an EM wavefront using such interface discontinuities was developed in [20]. Amidst the growing apprehension towards production and commercialization of metamaterials, it became evident that their 2D counterparts, metasurfaces, are the future facing technology that has potential for device development. A staggering number of trailblazing technology and applications have been proposed and demonstrated ever since the formulation of generalized Snell's laws [20].

Today, RF engineers and researchers focus more on developing controllable, programmable, digitally coded and intelligent metasurfaces [21–25]. The metasurface includes RF active components and electronic switches that allow its properties to be tailored to specific needs and applications. Meta-atoms can actively or passively change their state and are made to look like digital bits [7,26]. The ideas behind metasurfaces have progressed to the point where self-adaptive and cognitive metasurfaces are now possible [27]. Figure 1 gives a pictorial representation of how metasurfaces have evolved over the years.
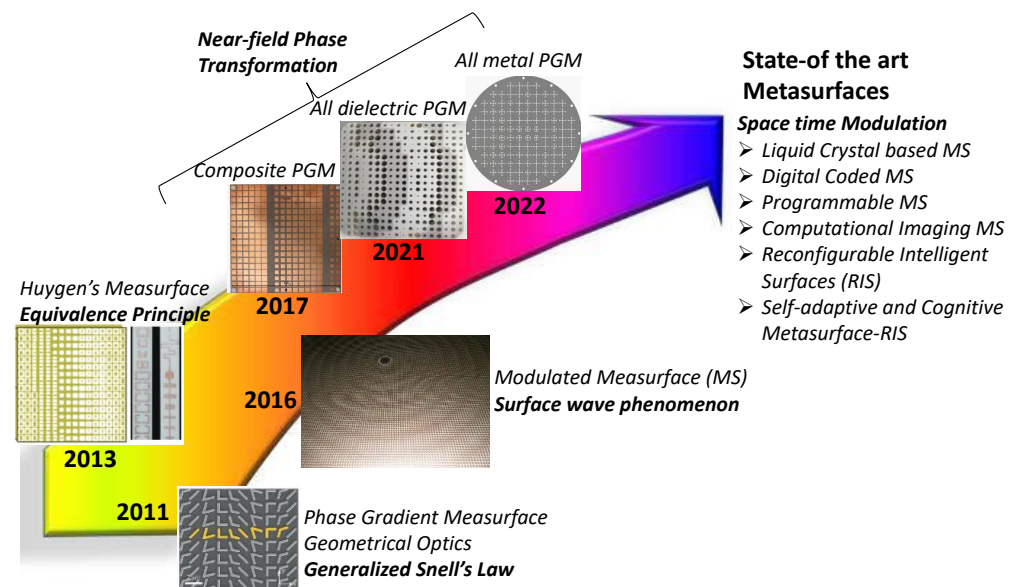

Figure 1. Evolution of metasurfaces over the last decade and some state-of-the-art metasurface technlogogies. The source for metasurface figures are as follows: 2011 [20], 2013 [9], 2016 [28], 2017 [29], 2021 [30] and 2022 [31]

1.4. Classification of Metasurfaces

Metasurfaces can be broadly divided into two categories: *homogeneous metasurfaces* and *inhomogeneous metasurfaces*. When a metasurface is composed of a periodically arranged array of identical unit cells in xy-plane, the propagation constant is uniform over the entire surface area. This structure is known as a homogeneous metasurface. Unit cell size and metasurface periodicity are often subwavelength; therefore, a homogeneous metasurface transmits or reflects plane waves like a homogeneously polarized sheet [32]. Such metasurfaces can be used to manipulate the key parameters of EM waves, which are phase, amplitude and polarization, either passively or actively. The second category includes 2D structures with non-identical subwavelength inclusions referred to as "meta-atoms" (also known as unit-cells, phase-transforming cells or phase-shifting cells) arranged in a specific "macro-order". Hence, they are locally non-periodic and called inhomogeneous

metasurfaces. The macroscopic order can be tailored to achieve a desired gradual variation in surface properties to realize several functionalities, such as metalenses, meta-holograms, metasurface-based cloaking, unique beam generation, and tunable inhomogeneous metasurfaces. One of the subcategories of inhomogeneous metasurfaces is *gradient metasurfaces (GMs)* [2]. They have incremental phase discontinuity and are characterized by a transversely inhomogeneous surface impedance profile. Such inhomogeneous synthetic surfaces exhibit spatially varying amplitudes, phases and polarization of scattered fields. These locally non-periodic gradient metasurfaces are capable of anomalous reflection and refraction, which significantly enhances their wave molding capability in both near-field and far-field, with an increased degree of freedom, large efficiency and minimal footprint. A set of distinct meta-atoms are arranged to form a supercell that is periodically repeated to create a complete metasurface. They exhibit transverse variation in their surface impedance profile. In fact, these in-homogeneous gradient metasurfaces are a bridge between propagating waves and surfaces waves since a gradient phase profile can be exploited to couple propagating waves to surface waves with a 100% efficiency [33].

Metasurfaces are also classified based on the fundamental response of its constituent elements to excitation. If a metasurface can support either only electric surface currents or only magnetic surface currents, they are termed *electrically polarizable metasurfaces* and *magnetically polarizable metasurfaces*, respectively [34]. Metasurfaces with non-zero thickness magneto-electric sheets that supports both electric and magnetic surface currents are known as *electrically and magnetically polarizable metasurfaces* [35]. Linear metasurfaces where both electric and magnetic polarizations can be induced by both incident electric and magnetic fields are known as *bianisotropic metasurfaces* [36]. Furthermore, there are metasurfaces that can simultaneously control reflection and transmission of incident EM wave together with the surface waves travelling along the metasurfaces. These are referred to as *metasurfaces for surface wave control* and they have opened a new avenue of research known as *metasurfing* [37].

Two important sub-classes based on the topology that constitutes the metasurface was proposed in [38], namely metafilms and metascreens. Metafilms are the metasurfaces with *cremet* topology that indicates an array of isolated, non-touching scatterers [39]. Metascreens are the metasurfaces that have a *fishnet* structure and are composed of an array of apertures in a reflective, otherwise impenetrable sheet [40].

In this article we focus on metasurfaces for electromagnetic applications. Section 2 describes the design principle of thin artificial interfaces more widely known as metasurfaces. Section 3 discusses several methods available in literature for synthesis of electromagnetic metasurfaces. Materials used and fabrication methodlogies preffered based on the choice of materials is explained in Section 4. Various types of meta-atoms (or unit cells) used for the design of EM metasurfaces are critically analyzed and discussed in Section 5. Section 6 the applications of metasurfaces in electromagnetics. Section 7 summarized the work with several open questions and inferences.

2. Design Principle

Classical optics assumes that a physical interface acts as an ideal boundary condition and does not change the properties of impinging EM waves. Snells' laws of reflection and refraction form the basis for geometrical optics, which states that behaviour of a light beam at the interface between two media is completely determined by the refractive indices of these two media according to:

$$\begin{cases} \sin \theta_i = \sin \theta_r \\ n_1 \sin \theta_i = n_2 \sin \theta_t \end{cases} \tag{1}$$

where θ_i is the angle of incidence in medium 1 with refractive index n_1, θ_r is the angle of reflection in medium 1, and θ_t is the angle of refraction in medium 2 which has a refractive index of n_2.

Metasurface synthesis based on generalized Snell's laws can be dated back to 2011 when Capasso and group revisited the classical Snell's laws to reformulate them for interface discontinuities [20]. Phase discontinuity introduced by artificial boundaries are expressed by generalized Snell's laws that apply Fermet's principle.

Figure 2 illustrates the difference (Only refracted wave is shown for brevity. A similar ray diagram can be made for reflection). When an EM wave propagating with an angle θ_i relative to the surface normal, meets an artificial interface, the behaviour of EM wave can be determined by generalized Snell's law (2), which considers propagating phase and abrupt phase introduced by the interface discontinuity:

$$\begin{cases} n_2 \sin \theta_t - n_1 \sin \theta_i = \dfrac{\lambda_\circ}{2\pi} \dfrac{d\phi}{dx} \\[2mm] \sin \theta_r - \sin \theta_i = \dfrac{\lambda_\circ}{2\pi n_1} \dfrac{d\phi}{dx} \end{cases} \tag{2}$$

where n_1 and n_2 are the refractive indices of the two mediums on both sides of the artificial interface, $\lambda_\circ$ is the free space wavelength, θ_i, θ_r and θ_t are the angles of incidence, reflection and refraction, respectively. The term $d\phi/dx$ is the gradient of phase discontinuity (in the plane of incidence) introduced in the incident EM wave by the artificial interface. If $d\phi/dx = 0$, Equation (2) becomes Equation (1), and we obtain the conventional Snell's laws with a continuity of in-plane wave vector. The generalized law of reflection and refraction overcomes the constraints imposed by the conventional Snell's law with a possibility to decouple incident, reflected and refracted angles. A further look into Equation (2) shows that for a given angle of incidence θ_i, there exists such value of the phase gradient term $d\phi/dx$ that results in parallel wave propagating with $\theta_t = 90°$. If $d\phi/dx$ is increased further, θ_t becomes a complex quantity at which point the refracted waves will vanish and plane wave will be converted to surface waves as explained in [33]. Based on generalized Snell's law, the local reflection and transmission coefficients of a PGM can be engineered such that the incident wave obtains a tangential momentum required to be locally rerouted towards the desired direction.
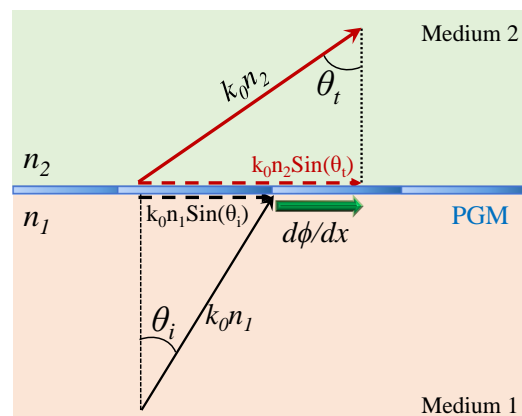

Figure 2. Generalized Snell's law (A 2D situation where the phase gradient lies along the plane of incidence). PGM referes to phase-gradient metasurface.

3. Methods of Synthesis

An efficient design technique is imperative to implement the metasurfaces to their full potential. Majority of electromagnetic metasurfaces which require high transmission are designed based on Huygen's principle [41]. An ideal gradient with continuously varying surface parameters can transform an EM wave with a 100% efficiency. Due to subwavelength nature of its constituent elements (meta-atoms or unit-cells), metasurfaces can be considered as infinitesimally thin sheets with arbitrary lateral extension and a tailored EM wave transformation can be achieved via generalized sheet transition condition (GSTC) [35,42]. Typically, realization of a metasurface is a two step process: (1) determine

a continuous mathematical transfer function for transverse variation of surface waves followed by discretization of the derived transfer function to obtain the subwavelength element corresponding to the transfer function at each position in the supercell (*macroscopic design*). (2) perform full wave parametric sweep to obtain the phase and magnitude lookup table to determine appropriate geometry of each unit-cell within the supercell to finally realize a complete 2D metasurface using periodic boundary conditions (*microscopic design*). Some analytical synthesis techniques introduced in the recent past have proven to be powerful and versatile tool for metasurface design [9,43–45].

3.1. Synthesis Based on Generalized Snell's Laws (The Phase-Shift Approach)

Metasurface synthesis based on generalized Snell's laws can be dated back to 2011 when Capasso and group revisited the classical Snell's laws to reformulate them for interface discontinuities [20]. In 2011, it was demonstrated that an artificial interface composed of an ensemble of V-shaped nano-antennas exhibits position dependent abrupt phase change $\Phi(x, y)$ for transmitted and reflected waves [20]. In this work the double resonance property of V-shaped antenna was exploited to achieve a full phase range from 0 to 2π with high amplitude. The concept of imparting controlled interfacial phase discontinuity along the path of wave propagation has been used in various metasurface designs based on generalized Snell's laws and (Panchratnam-Berry) PB phase [46] metasurface design based on spin-dependent generalized Snell's laws [47,48]. The phase profile required to achieve a desired aperture field is stipulated and the unit cells with unity transmission magnitudes and required phase shifts with respect to impinging field are arranged in a 2D array to design the complete metasurface [49].

Electrically large phase gradient metasurfaces with supercell periodicity are very common in antenna applications and they are often synthesised using near-field phase transformation method (essentially the same *phase-shift approach*) which also follows from generalized Snell's laws and uses highly transparent unit-cells with required phase delay obtained from a lookup table of scattering parameters. Details of near-field phase transformation method can be found in [29,50,51]. Some articles [35,52] drew the attention towards the limited efficiency of this method for extreme wave transformation and the trade-off that exists between efficiency and steering angle in canonical problems of plane waves steering. This drawback can be attributed to the impedance mismatch between incident and refracted wave which results in reduced efficiency and spurious scattering. The following two approaches can overcome these limitations by implementing exact boundary conditions to obtain desired surface impedance profile or surface susceptibility profile taking into account the existing mismatch.

3.2. Synthesis Based on Surface Impedance Tensor

Metasurfaces are electrically thin sheets (zero-thickness film) due to subwavelength nature of its fundamental building block (meta-atoms or unit-cells), and hence can be characterized by their surface impedance which depends on unit-cell geometry and supercell periodicity. If the supercell has subwavelength periodicity, only the fundamental Floquet modes propagates as a plane wave while the other higher order modes are evanescent and contribute towards surface impedance. Wave propagation constant depends on surface impedance. In order to achieve arbitrary EM field distributions both electric and magnetic surface currents must satisfy the transition conditions (field discontinuities). The ultra-thin metallic surface patterns are commonly used to realize electric surface impedance while metallic loops creates a magnetic surface impedance [53]. Scalar impedance metasurfaces provide full control over transmission and reflection properties of EM wave. Tensor impedance metasurfaces have enhanced ability to control polarization, spin Hall effects and are applied for far-field imaging, group negative refraction and lensing, surface waveguides, surface wave holographies, local density-of-states tailoring, spontaneous emission enhancement and illusion scattering [54]. The proportionality between tangential electric and magnetic field on one side of the surface defines the impenetrable surface impedance

while the relationship between tangential electric and magnetic field across the surface is termed as penetrable surface impedance [55]. An impedance relations between averaged surface current and tangential electric and magnetic field is established to characterize the metasurface.

The general recipe for surface impedance based metasurface synthesis has been elucidated by Pfeiffer and Grbic in [9,56,57]. To know more about GSTCs [40] and impedance tensor based metasurface synthesis, along with the derivation of mathematical expressions for calculations of electric sheet admittance and magnetic sheet impedance in terms of average tangential fields along the interface, readers are encouraged to read the work published in [58–61]. Another synthesis technique follows a similar approach from polarization perspective since transmissions and reflections dyadic are functions of polarizabilities of subwavelength inclusions (unit-cells) [43,57,62]. Modulated metasurface antennas have emerged as a captivating area of research in the last decade. An impedance-based approach towards amplitude synthesis of the aperture field distribution in modulated metasurface antennas is proposed and exemplified in [28].

3.3. Synthesis Based on Surface Susceptibility Tensor

Two different methods to synthesise metasurface for time-harmonic waves are discussed in [63] by Caloz and group. In the first method spectral conservation of momentum was implemented to scalar and paraxial wave transformation problems. However, extending their application to vectorial problems involves further complex analysis which makes the implementation difficult [64].

Second proposed method involves direct spatial approach to extract susceptibility tensor of metasurface which is later implemented by the same authors in 2015 [45] for the synthesis of metasurfaces to transform arbitrary incident waves to arbitrary reflected and transmitted waves. The metasurfaces are characterized by spatial surface susceptibility tensors related to incident, reflected and transmitted waves via GSTCs. This method is intrinsically vectorial hence more suitable for beyond paraxial (full vectorial) EM problems. It provides closed-form expressions relating surface susceptibilities and scattering parameters calculated with periodic boundary conditions and is therefore extremely fast. Synthesis involves determining exact tensorial susceptibility function for the metasurface while realization involves full wave EM simulations to find the scatterers (unit-cells) with appropriate susceptibility based on S-parameter. The mathematical expression and implementation detailed are not included in this manuscript for brevity and the inquisitive readers are advised to read [65–69].

3.4. Synthesis Based on Diffraction Grating Method (Meta-Grating)

Rerouting an incident wave towards an arbitrary direction with a 100% efficiency without spurious diffraction can be achieved by complex transverse metasurfaces [66] which exhibit either mono-isotropy with loss and gain, non-reciprocity [70] or bianisotropy [71]. However, these configurations suffer from implementation difficulty in terms of fabrication resolution. Recent studies show that PGMs emulate the behaviour of a blazed grating [72]. A new concept of meta-gratings based on classical diffraction grating principle was proposed by Ra' di and group for extreme wavefront transformation [73]. It opened up an interesting alternative to synthesise metasurfaces. Several metasurfaces based on the concept of metagrating were later reported in [74,75]. Metagratings are engineered to cancel spurious propagating diffraction orders and allow the desired ones, by exploiting the well-established physics of a periodic grating. A 1D metagrating is analogous to periodic array of supercells composed of *N* thin wires each and hence is analyzed by using theory of diffraction of plane waves by periodic arrays. It is imperative to mention that the inter-wire distance is in the orders of operating wavelength λ. The diffraction angles of Floquet-Bloch modes can be found using grating formula given in the equation below:

$$L(\sin\theta_m - \sin\theta_i) = m\lambda \tag{3}$$

where m is the diffraction order number, θ_i is the angle of incidence, and L is the period of the array (length of supercell). Thus, it is evident that by suitably tailoring the local period and the electromagnetic response of each wire (which in practice are implemented using subwavelength unit cells in the metagrating) one can control the number of diffraction orders. For an incident wave, the scattered waves are represented by a set of Floquet-Bloch modes that depend on the period of the array (length of supercell). Metagratings overcome the efficiency limitations and complex fabrications which is otherwise experienced with PGMs. In [76], a simple varactor diodes based re-configurable metagrating was proposed and implemented at microwave frequency. It is an important precursor for a new generation of re-configurable microwave devices that enable a dynamic and exceptional control over transmitted and reflected diffraction patterns. Additionally, metagratings do not need to provide a gradient impedance profile to reroute the incident wave. Hence, their realization is comparatively more straightforward than graded metasurfaces. The elaborate theory of metagrating and its implementation can be found in some astounding works reported in [73,77–79].

4. Materials and Fabrication Methods

The choice of materials in implementing EM metasurfaces significantly impacts physical and electrical performance. This also determines the success of the prototypes intended for particular RF applications. The associated cost, design and fabrication complexity are also attributed to the materials used to design metasurfaces. Over the past, different types of metasurfaces have been successfully investigated based on various synthesis methods discussed in Section 2. In this direction, in the literature, metasurfaces are typically made of all-dielectrics, composite or fully metallic materials in the RF domain.

Under the first group, as shown in Figure 3a, metasurfaces are synthesized using fully dielectric materials. In the 3D versions, thick and bulky dielectric blocks are typically used to develop metasurfaces for various RF applications, requiring expensive and sophisticated machining tools and techniques for fabrication [80]. Recently, the 3D printed technology advanced all-dielectric metasurfaces even further by using low-cost tailored dielectrics and in-house rapid prototyping facilities [30]. Unlike conventional RF laminates, the dielectric constant (effective permittivity) can be modulated locally simply by implementing the air inclusion or by varying the in-fill percentage in the printing process [81]. Due to the need for discretized phase shifts, such all-dielectric metasurfaces preferably well choose to be synthesized via the phase-shifting approach. All-dielectric metasurfaces have also been realized using susceptibility tensors [82].
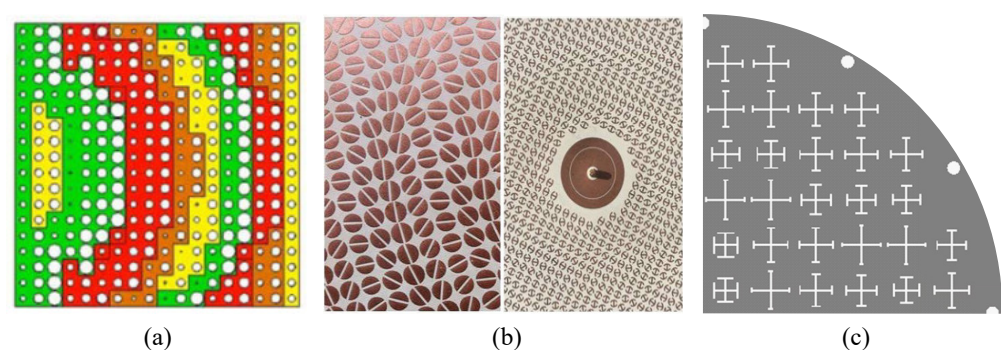

(a)   (b)   (c)

Figure 3. Front layouts of metasurfaces developed on (**a**) all-dielectric (color indicates variable dielectric constants) [30], (**b**) composite (different metal shapes printed on dielectrics) [83] and (**c**) fully metallic materials (slots are created in thin monolithic metal sheets) [31].

The metasurfaces in the second group are typically made of different shapes of periodic metallic patterns printed on single or multilayer dielectric substrates and sandwiched together to make a single one, as shown in Figure 3b. Through the use of a surface impedance and susceptibility tensor approach, GSTCs or homogenized boundary conditions (BCs),

such printed metasurfaces can be efficiently designed [28,37,38,45,47,58,66,67,84]. One can modify the BCs spatially by changing the shape, orientation or geometric dimensions of the printed patterns in the host dielectric substrates while keeping the meta-atom size fixed [83]. In addition, phase-shifting and array theory approaches have also been widely investigated to develop printed metasurfaces for different RF applications [29,72,85,86]. In the latter case, the incident EM waves are modulated locally by discrete meta-atoms derived through Floquet-mode analysis. The composite metasurfaces are relatively thin, light and easy to fabricate using low-cost printed circuit board (PCB) technology.

However, despite having industry-grade performance, the all-dielectric or dielectric-loaded metasurfaces suffer from dielectric losses, especially in high radio-frequency applications, whereas low-loss dielectrics are costly. Moreover, they are limited in high-power applications with a possibility of dielectric breakdown or space applications due to environmental stress such as ionization, carbonization or cryogenic temperature issues. On the other hand, all-metal metasurfaces in the third category eliminate dielectrics, as shown in Figure 3c. They can be made of thin, light metal sheets and are applicable even in space and high-power microwave applications where high-power or extreme temperature variations are expected [31,87–90]. Depending on the proposed metallic architecture, such metasurfaces can be fabricated using commercially available low-cost metal manufacturing facilities, including computer numerical control (CNC) machining, plasma cutting, metal additive manufacturing, waterjet cutting, metal stamping and laser cutting. Furthermore, metals are far less expensive than low-loss RF laminates, and no bonding technique is required, resulting in lower production costs. Such metasurfaces are mainly synthesized based on generalized Snell's laws, the phase-shifting approach, and classical array theory. A separate family of plasmonic metasurfaces operate at high frequencies where metals sustain states propagating along, and tightly bound to, metal-dielectric interfaces while exhibiting relatively low dissipation losses and resonance-enabled potential for arbitrary control over the amplitude, phase, direction and polarization of their impinging wave [91].

5. Design and Optimization

5.1. Meta-Atoms: Microscopic Units of Metasurface

The fundamental elements for metasurfaces commonly known as meta-atoms (also called unit cells, phase-shifting cells) have to be carefully designed to have near-perfect transmission (or reflection in the case of reflective metasurfaces) characteristics. For instance, in order to designing transparent phase gradient metasurfaces a full phase range of 360° with high transmission efficiency is required. Several topologies have been investigated to design efficient metasurfaces considering transmission characteristics, bandwidth, oblique incidence sensitivity, design complexity and ease of mass manufacturing. Some common unit cell topologies that have been widely used in designing metasurfaces using phase-shift approach are listed below:

- Composite meta-atoms which are single or multi-layer structures with metallic patches sandwiched between layers of dielectrics. The metallic patches can have various shapes such as circular, square, circular-ring, square ring, circular or square patch inside a wireframe, Jeruselem cross, Swastika and flange shaped or a combination of these. The size of the meta-atom is usually kept less than or equal to half wavelength. The metallic patch pattern is varied along x, and/or y direction to achieve a desired phase and amplitude profile in the near-field.
- All dielectric (metal-less) meta-atoms which are essentially a block of substrate. It may sometimes have a through hole (for example square or circular or cross slots). The phase delay is varied either by changing the height of the meta-atom or the permittivity of the substrate used. Delay in transmission phase is proportional to height as well as the permittivity of the dielectric material used. An all-dielectric metasurface can be easily fabricated using 3D printing technology.
- All-metal meta-atoms are composed of single or multi-layer metal sheets with slotted patters. Several types of slots' shapes that have been successfully implemented to

design planar, lightweight fully metallic metasurfaces include modified-eight-arms-asterisk (MEAA) slot, Jerusalem slot (JS), Swastika slot (SS). Such slots-in-sheets (SiS) design approach avoids the 3D metallic structures and also confirms the mechanical robustness of the metasurface [31,87,88].

Huygen's metasurfaces intuitively used wire/loop unit cells in their stages of infancy. However, this field has matured since and several unit-cell designs such as omega-shaped patterns, spiral-shaped patterns including cascaded multi-layer unit cells have widely experimented and used. The capacitive and inductive properties of stacked metallic patterns are used to synthesis desired values of impedance and admittance reactances [92].

Another approach of designing metasurfaces involves determining the spatial distribution of the sheet impedance tensor or sheet susceptibility tensor for each metasurface layer in the cascade using GSTCs, as explained earlier in Sections 3.2 and 3.3. The subwavelength elements are printed on a grounded dielectric slab and topologies that have been widely used in designing metasurface antennas based on surface impedance tensor method includes coffee bean shaped patch, split ring resonators, coffee bean, patch with slot, grain of rice, patch with cross slot, double π and double anchor [83]. These unit cell elements are generally of the size between $\lambda_0/10$ $\lambda_0/5$ and essentially behave like pixels in a black and white printed image. Metasurfaces that use simple canonical metallic shapes generally have larger bandwidths [93].

Standard configurations of unit cells noted in the design of metagratings include an array of loaded metallic strips, omega dipoles or electric dipoles, fish-shaped multipolar single element, bianisotropic meta-molecule supporting four resonances, single high-index dielectric cylinder, elliptical hollow cylinders carved periodically in a steel background, silicon rods with different sizes, N polarization electric line currents per unit cell, multilayer multi-element metagratings which enable higher degrees of freedom such as multilayered loaded-wire metagrating, and reconfigurable metagratings based on graphene [78,79]. Microelectromechanical systems (MEMS) based programmable and smart metasurfaces, Microfluidic technology based fluidic metasurfaces, fluid-background metasurface (a solid-liquid mixed metasurface) and metasurface on fibre are some of the upcoming technologies where the unit cells are and various innovative unit cells are used in these designs. However, the details are not provided for brevity.

5.2. Optimization

Despite the remarkable progress in the design framework, metasurface optimization remains an exhilarating topic hereafter. Strict design and performance requirements in advanced realms of technology necessitates optimization of metasurface based systems to maximize the metasurface efficiency. Metasurfaces are often electrically large with thousands of small inclusions/features and their simulations using conventional numerical methods incur high computational costs. Choice of geometry and material for unit cell design involves time-consuming parameter search to build a lookup table. However such parameter sweeps do not account for near-field interactions (mutual coupling) that strongly influence the device performance. Besides, optimization over a large parameter space is complex. Dedicated electromagnetic CAD tools combined with suitable optimization strategies are needed to meet such immense computational challenges. New and advanced method such as inverse design, neural network and machine learning techniques could potentially extend the capabilities of metasurfaces.

Some articles reported in the recent past have attempted to make these problems more computationally tractable by exploiting the periodic nature of metasurfaces [72,94]. Optimization is implemented to a smaller sub-section (supercell) of metasurface and the full surface is then designed by periodically repeating the optimized sub-sections. Thus, the computational complexity of the optimization is reduced from high-polynomial to linear. Both local and global search strategies have been exploited. With a good initial parameter guess, local methods such as topology optimization provide rapid convergence to local minima/maxima. On the other hand, global methods like genetic algorithm (GA)

and evolutionary algorithms (EA) implement stochastic search technique and guarantee a global or near global optimum. Evolutionary algorithms are highly efficient in handling large parameter space optimization as it supports parallel computation. A metasurface is optimized based on multi-element phase cancellation method using particle swarm optimization in [95] for ultra-wideband radar cross-section (RCS) reduction. Other significant efforts towards metasurface optimization can be found in [85,86,96]. Oftentimes the isolated behaviour of optimized supercell is different than when stitched together to form a complete surface. This is primarily due to the fact that simpler subsection optimization considers infinite periodicity whereas in reality the metasurfaces have finite dimension. Mutual coupling and edge effects are hard to model in the available EM solvers. In [97], a summary of recently proposed optimization methods for phase-gradient metasurfaces is presented. Based on the objective function, the optimization methods were categorized as, radiation pattern-based optimization and Floquet-mode-based optimization. Both methods exploit periodicity and use simpler equivalent models to reduce the computation complexity multiple folds. They also take into account the variations in mutual coupling between dissimilar adjacent cells in a supercell during the process of optimization.

6. Applications of Metasurfaces

To date, metasurfaces have been widely used in the area of optics, electromagnetics as well as acoustics. However, we avoid discussing the applications in optics and acoustics for brevity as they are beyond the scope of this article. Some of the electromagnetic functionalities of metasurfaces are spectrum filtering [98], engineered beam refraction and/or reflection [99], controlled absorption [100], cloaking [101], surface electromagnetic wave couplers, plane wave to surface wave conversion [102], energy harvesting using graded metasurfaces [103] and encoding for secure communication [104]. In antenna applications, metasurfaces are used for improving bandwidth and enhancing antenna gain [105,106], beam splitting [107], beam steering [29], multi-beam scanning [108], advanced radiation pattern molding [71], beam focusing [109], polarization manipulation [110], collimating leaky waves in high gain planar antenna and acting as superstrates in high gain low profile antennas [111].

Some of the recently found applications of metasurfaces in electromagnetics include, anti-reflection coating, phase shifters, stable beam traction, analog computing, coherent perfect absorption, imaging beyond diffraction limit, ultra-thin black-body absorber and Bessels's beam generator [24]. They can be applied for intelligent transportation systems,Vehicular Communications, Internet of Things (IoT) networks in moving platforms such as spacecraft and drones, unmanned aerial vehicle (UAV)-based wireless communication, and simultaneous wireless information and power transfer systems. Some of the future facing applications are next generation imaging, sensing and quantum information processing. Metasurfaces for smart electromagnetic platforms are known as intelligent metasurfaces and are capable of digitalization, programmability, and intelligence [112]. Metasurface-based smart systems when integrated with detection, artificial neural networks, and feedback systems are expected to play an important role in wireless communications, advanced sensing technologies and artificial intelligence.

Other applications of metasurfaces to antennas include but are not limited to, synthetic aperture radar (SAR) imaging with dynamic metasurfaces [113], remote/wireless sensing [114], microwave imaging for tumour detection [115], spatial filters [116], telemetry and tele-command of deep-space missions [117], reconfigurable antenna design, frequency scanning metantennas [118], energy harvesting [119], wearable metasurface enabled antenna for medical implants [120], future applications such as chiral quantum metasurface-based antennas, computational microwave and through-wall imaging [113] and frequency-diversity imaging [121]. Metasurfaces open another very fascinating approach towards integrating solar cells with antennas, which has potential applications in autonomous communication systems and CubeSats. Such powerful combination of solar-cells with antennas could be

very beneficial for self-sustaining wireless devices, radio frequency identification (RFID) and the Internet of Things (IoT) [122,123].

6.1. Metasurfaces for Linearly Polarized EM Waves

The metasurfaces discussed in this section worked devotedly for linearly polarized EM waves. The fundamental building blocks for all the below mentioned metasurfaces are planar resonating meta-atoms. The first gradient metasurface realized using eight distinct V-shaped nano-antennas of varying size, direction and opening angle could tilt the transmitted EM wave to a pre-defined direction by providing desired phase pattern over the surface at both mid-infrared [20] and near-infrared frequencies [124]. Despite exceptional wave transforming abilities along with a full 360° transmission phase coverage, the V-shaped nano-antenna based metasurface exhibits only partial anomalous refraction which significantly reduced their efficiency.

An alternative approach based on reflection geometry and MIM (metal-insulator-metal) meta-atoms [33] was used to enhance the efficiency of gradient metasurfaces. A highly efficient reflection-type gradient metasurface composed of H-shaped MIM meta-atoms that inherently support a 100% anomalous reflection efficiency was demonstrated and fabricated exhibiting as high as 80% efficiency in the near-infrared regime [124]. The reflection based approach was still unsuitable for many other applications since the feed for reflecting gradient metasurfaces block the radiated wave. A high efficiency gradient metasurface based on the concept of Huygen's surfaces was proposed where the meta-atoms were meticulously engineered to obtain a 100% transmission amplitude and a linear varying phase covering entire 360° phase range. A maximum efficiency of 86% was obtained in such Huygen's metasurfaces [9].

An array of C-shaped split rings resonators with constant amplitude and linearly varying phase profile were used to design a gradient metasurface at 1 THz to obtain a maximum beam tilt of 84° [125]. Digital metasurface designed by Cui et al. used meta-atoms with discretized phase values and their functionalities were extended to beam-manipulation and scattering reduction [126,127]. In 2015, a simple yet elegant metasurface composed of trapezoidal shape silver antenna array was designed by Li et al. which provided quasi-continuous full range (2π) reflection phase and extremely high amplitude with 85% efficiency. The metasurfaces discussed in this section could only support linear polarization and also exhibited drawbacks such as frequency dispersion, limited bandwidth and fabrication complexity.

6.2. Metasurfaces for Circularly Polarized EM Waves

A completely new strategy for metasurface design was explored after realizing the limitations of resonance based linearly polarized metasurfaces. An assembly of identical sub-wavelength elements (unit-cell) with varying orientation angles are used for meta-surface design. The varying phase is governed by the orientation angle of each unit-cell which holds the ability to mould the wavefront of a circularly polarized wave [46]. When a circularly polarized (CP) wave is incident on such unit-cells, it excites electric field in orthogonal directions with a phase difference of 90°. Such anisotropic nature bespeaks the existence of both spin-conserved and spin-reversed components of CP wave that generates a spin-dependent diffraction known as photonic spin Hall effect (PSHE).

The groundbreaking discovery by Pancharatnam in the year 1956 [128], unveiled that the spin-reversed component carries an additional phase of exp $j2\theta$ corresponding to $\theta°$ rotation of the resonator. Such phase was later interpreted as geometrical phase by Berry [129]. The first Pancharatnam-Berry (PB) phase metasurface design based on the concepts developed in [128,129] used an array of identical sub-wavelength dielectric gratings with periodically varying orientation angle [46]. Another startling contribution was made in 2011 by Hasman and group were they report the use of coupling-induced anisotropy in a curvilinear array of circular apertures drilled in a gold plate to create PSHE. The work done in [130] succinctly encapsulates the concept of PB phase along with a

description of spin-dependent generalized Snell's law. Despite growing interest, the PB devices failed to achieve high efficiency which was theoretically limited to a maximum of only 25% [131] and the same was later manifested in the design reported in [132].

An increase in efficiency was indispensable to extend the applicability of PB phase metasurfaces. A high efficiency (nearly 80%) PB phase metasurface for holography was designed using meta-atoms that satisfied a similar criterion [133]. In 2017, Luo and group made a tedious effort to design a PB metasurface in transmission geometry with a 100% efficiency by exploring the possibility of inducing both electric and magnetic response withing the meta-atom [134]. Some other significant recent contributions are [29,135–137]. A multi-layer metasurface can simultaneously increase the gain and transform linear polarization to circular polarization in a patch antenna. Thus, metasurfaces have been implemented in the design of several single and multi-band, high-gain, CP antennas [138,139].

6.3. Metasurfaces for Near- and Far-Field Synthesis

Near-field phase transformation in an aperture-type antenna (resonant cavity antenna) was incorporated by placing a pair of rotating phase gradient metasurfaces close to and above the antenna to steer the beam in a conical range with an apex angle of 102° in [29]. Metasurfaces can mimic a perfect magnetic conductor or a perfect electric conductor within a particular frequency range [140]. Thus, most low-profile antenna systems have replaced metallic reflectors placed quarter-wavelength below the antenna radiator with metasurfaces placed in very close proximity, with perfectly matched impedance assisting in unidirectional radiations.

Electrically large metasurfaces are very common in antenna applications and they are often synthesised using near-field phase transformation method (essentially the same *phase-shift approach*) which also follows from generalized Snell's laws and uses highly transparent meta-atoms with required phase delay obtained from a lookup table of scattering parameters, to synthesize a desired near-field phase profile (for example Figure 4a. Details of near-field phase transformation method can be found in [29,50,51]. This method is used to design metasurface lens [107,141], phase correcting surfaces [87,88], radar cross section reduction surfaces [142], beam steering antennas [31,72,85] and beam-splitting antennas [26]. This approach has recently been successfully re-explored to create antenna technology that can steer the quasi-non diffractive beam over a large range of angles, from 0 to 54° in the zenith, with a stable depth of field view [143]. Near-field imaging technology and wireless power transmission are potential sectors to use such antenna systems.
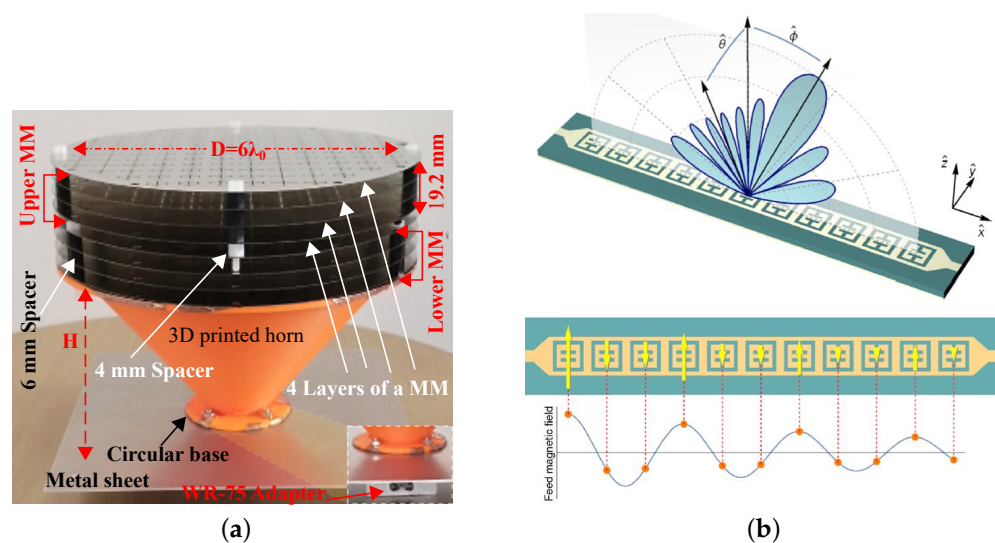

(a)   (b)

Figure 4. Metasurface-based beam-steering antennas. (**a**) 2D beam-steering antenna system driven by a pair of metallic metasurfaces [31]. (**b**) Metasurface antenna and illustration of the excitation by the feed wave [144].

Focusing metasurfaces with hyperbolic phase distributions are a prominent choice for the design of high-gain antennas due to their planar profile, easy fabrication, and excellent beam control [145]. A multi-layered PGM was used to design a high-gain lens antenna for X-band applications in [146]. The Huygens' metasurfaces-based lens is found to extend the angular scan range of phased arrays in [61,147]. It is important to understand that, PGMs are non-radiating and need a base antenna to operate (Figure 5a) whereas metasurface antennas as shown in Figures 4b and 5b are self-radiating.
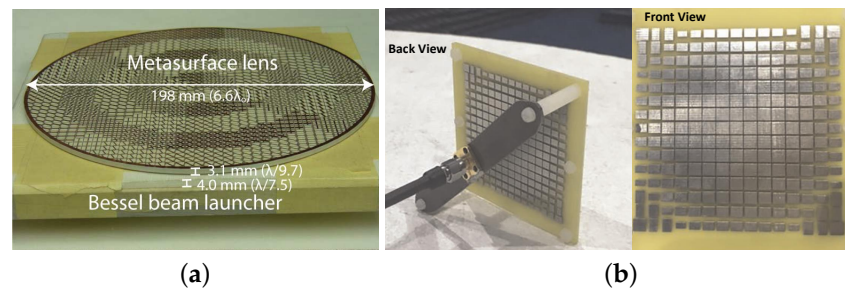

| (a) | (b) |

Figure 5. Metasurface for high-gain antennas. (**a**) A circularly polarized metasurface lens placed on top of the Bessel beam launcher [147]. (**b**) PGM based high gain lens antenna [148].

7. Discussion

Metasurfaces are unequivocally excellent spatial processors with exotic surface waves that strongly enhance their EM wavefront control capabilities leading to fascinating physical effects and versatile applications. They are a promising candidate for real-world solutions. Recent years have seen significant advancement of metasurfaces in almost all regimes of electromagnetics and optics that has been elucidated in numerous review articles from different perspectives and areas of application. In this article, we focus on the story behind the discovery, evolution and exponentially growing popularity of metasurfaces in almost all areas of application that an inquisitive human mind can think of. The history of metasurfaces started with the birth of metamaterials to surpass the abilities of naturally existing materials, followed by the advent of metasurfaces to address the limitations of metamaterials, and the world since then has seen several disruptive, trailblazing technologies that aim to achieve unprecedented control over the properties of EM wave. The metasurfaces expanded in various realms and are classified broadly in this article to provide more clarity. The in-depth understanding of physics and EM wave phenomenon at artificial boundaries/interfaces led to easy synthesis techniques which are encapsulated and briefly discussed. A critical analysis is made based on the study of materials and manufacturing methodology used for design of metasurfaces. An evaluative deduction is provided on optimization techniques developed and implemented in metasurface design. Several applications of electromagnetic metasurfaces are highlighted and broadly classified. The article in its entirety provides a detailed understanding of metasurfaces in general and can help the new researchers make an educated decision for application-specific metasurface designs.

The design and fabrication of metasurfaces is often very complex and lacks precision due to multi-layer profile and small complex sub-wavelength inclusions. Using PCB technology, it might be possible to affordably prototype composite metasurfaces and metasurface antennas. In contrast, the 3D printed technolgy could be the best choice for low-cost in-house fast prototyping. The metallic metasurfaces could also be low-cost alternatives with a broader spectrum from space to high-power applications. Implementation of metasurface concept to curved surface are a foreseeable challenge for conformable and aerodynamic applications. This indirectly begets extension of creeping-wave theory to curved metasurface coated surfaces. No significant work is done in this direction until now and would need sizable effort. Metasurfaces with integrated active devices are more reliable and efficient in terms of losses and performance as opposed to discrete active devices. However, large scale implementation of such integrated devices needs excellent

accuracy and repeatability in the fabrication process. Lately, the interest has shifted to tunable metasurfaces-based beam steering antennas that allows real-time reconfiguration of phase distributions to achieve continuous beam steering. At microwave frequency, field programmable metasurfaces provide real-time and powerful beam manipulation capabilities. Using tunable materials and micro-electro-mechanical systems (MEMS) in conjunction with field-programmable metasurfaces enable similar abilities at terahertz frequency. However, non-linearity or breakdown associated with active metasurfaces can generate unwanted harmonics and grating or side lobes in radiation pattern due to self-steering tendency at high power. Mechanical varactors and MEMS devices can decrease the non-linearity to some extent. Advanced liquid crystals or ferro-electric materials also hold a similar potential. Nonetheless, most of these results are theoretical and lack experimental verification and optimization. Metasurfaces opens up another very fascinating approach towards integrating solar cells with antennas that have potential application in autonomous communication systems, as well as space communication systems (CubeSats). Investigations made so far in field of metasurfaces have revealed several challenges and open questions that call for more research to be conducted. We are collectively moving towards a new generation of smart devices with metasurfaces forming the backbone of the technology.

References

1. Quevedo-Teruel, O.; Chen, H.; Díaz-Rubio, A.; Gok, G.; Grbic, A.; Minatti, G.; Martini, E.; Maci, S.; Eleftheriades, G.V.; Chen, M.; et al. Roadmap on metasurfaces. *J. Opt.* **2019**, *21*, 073002. [CrossRef]
2. Ding, F.; Pors, A.; Bozhevolnyi, S.I. Gradient metasurfaces: A review of fundamentals and applications. *Rep. Prog. Phys.* **2017**, *81*, 026401. [CrossRef] [PubMed]
3. Chang, S.; Guo, X.; Ni, X. Optical metasurfaces: Progress and applications. *Annu. Rev. Mater. Res.* **2018**, *48*, 279–302. [CrossRef]
4. Chen, H.T.; Taylor, A.J.; Yu, N. A review of metasurfaces: Physics and applications. *Rep. Prog. Phys.* **2016**, *79*, 076401. [CrossRef]
5. Zang, J.; Correas-Serrano, D.; Do, J.; Liu, X.; Alvarez-Melcon, A.; Gomez-Diaz, J. Nonreciprocal wavefront engineering with time-modulated gradient metasurfaces. *Phys. Rev. Appl.* **2019**, *11*, 054054. [CrossRef]
6. Bukhari, S.S.; Vardaxoglou, J.Y.; Whittow, W. A metasurfaces review: Definitions and applications. *Appl. Sci.* **2019**, *9*, 2727. [CrossRef]
7. Liu, C.; Ma, Q.; Luo, Z.J.; Hong, Q.R.; Xiao, Q.; Zhang, H.C.; Miao, L.; Yu, W.M.; Cheng, Q.; Li, L.; et al. A programmable diffractive deep neural network based on a digital-coding metasurface array. *Nat. Electron.* **2022**, *5*, 113–122. [CrossRef]
8. Sun, S.; He, Q.; Hao, J.; Xiao, S.; Zhou, L. Electromagnetic metasurfaces: Physics and applications. *Adv. Opt. Photonics* **2019**, *11*, 380–479. [CrossRef]
9. Pfeiffer, C.; Grbic, A. Metamaterial Huygens' surfaces: Tailoring wave fronts with reflectionless sheets. *Phys. Rev. Lett.* **2013**, *110*, 197401. [CrossRef]
10. Lamb, H. On the reflection and transmission of electric waves by a metallic grating. *Proc. Lond. Math. Soc.* **1897**, *1*, 523–546. [CrossRef]
11. Wood, R.W. On a remarkable case of uneven distribution of light in a diffraction grating spectrum. *Proc. Phys. Soc. Lond.* **1902**, *18*, 269. [CrossRef]
12. Senior, T. Approximate boundary conditions. *IEEE Trans. Antennas Propag.* **1981**, *29*, 826–829. [CrossRef]
13. Marconi, G.; Franklin, C.S. Reflector for Use in Wireless Telegraphy and Telephony. US Patent 1,301,473, lApril 22, 1919.
14. Vogel, P.; Genzel, L. Transmission and reflection of metallic mesh in the far infrared. *Infrared Phys.* **1964**, *4*, 257–262. [CrossRef]
15. Veselago, V.G. The Electrodynamics of Substances with Simultaneously Negative Values of ϵ and μ. *Physics-Uspekhi* **1968**, *10*, 509–514. [CrossRef]
16. Ebbesen, T.W.; Lezec, H.J.; Ghaemi, H.; Thio, T.; Wolff, P.A. Extraordinary optical transmission through sub-wavelength hole arrays. *Nature* **1998**, *391*, 667–669. [CrossRef]

17. Pendry, J.B. Negative refraction makes a perfect lens. *Phys. Rev. Lett.* **2000**, *85*, 3966. [CrossRef]
18. Luo, X.; Ishihara, T. Surface plasmon resonant interference nanolithography technique. *Appl. Phys. Lett.* **2004**, *84*, 4780–4782. [CrossRef]
19. Xu, T.; Wang, C.; Du, C.; Luo, X. Plasmonic beam deflector. *Opt. Express* **2008**, *16*, 4753–4759. [CrossRef]
20. Yu, N.; Genevet, P.; Kats, M.A.; Aieta, F.; Tetienne, J.P.; Capasso, F.; Gaburro, Z. Light propagation with phase discontinuities: Generalized laws of reflection and refraction. *Science* **2011**, *334*, 333–337. [CrossRef] [PubMed]
21. Ma, Q.; Gao, W.; Xiao, Q.; Ding, L.; Gao, T.; Zhou, Y.; Gao, X.; Yan, T.; Liu, C.; Gu, Z.; et al. Directly wireless communication of human minds via non-invasive brain-computer-metasurface platform. *arXiv* **2022**, arXiv:2205.00280.
22. Tang, W.; Chen, M.Z.; Dai, J.Y.; Zeng, Y.; Zhao, X.; Jin, S.; Cheng, Q.; Cui, T.J. Wireless Communications with Programmable Metasurface: New Paradigms, Opportunities, and Challenges on Transceiver Design. *IEEE Wirel. Commun.* **2020**, *27*, 180–187. [CrossRef]
23. Ma, Q.; Xiao, Q.; Hong, Q.R.; Gao, X.; Galdi, V.; Cui, T.J. Digital Coding Metasurfaces: From Theory to Applications. *IEEE Antennas Propag. Mag.* **2022**, *64*, 96–109. [CrossRef]
24. Barbuto, M.; Hamzavi-Zarghani, Z.; Longhi, M.; Monti, A.; Ramaccia, D.; Vellucci, S.; Toscano, A.; Bilotti, F. Metasurfaces 3.0: A New Paradigm for Enabling Smart Electromagnetic Environments. *IEEE Trans. Antennas Propag.* **2021**, *70*, 8883–8897. [CrossRef]
25. You, J.W.; Ma, Q.; Lan, Z.; Xiao, Q.; Panoiu, N.C.; Cui, T.J. Reprogrammable plasmonic topological insulators with ultrafast control. *Nat. Commun.* **2021**, *12*, 5468. [CrossRef] [PubMed]
26. Ahmed, F.; Afzal, M.U.; Singh, K.; Hayat, T.; Esselle, K.P. Highly Transparent Fully Metallic 1-Bit Coding Metasurfaces for Near-Field Transformation. In Proceedings of the 2022 16th European Conference on Antennas and Propagation (EuCAP), Madrid, Spain, 27 March–1 April 2022; pp. 1–4.
27. Ma, Q.; Bai, G.D.; Jing, H.B.; Yang, C.; Li, L.; Cui, T.J. Smart metasurface with self-adaptively reprogrammable functions. *Light Sci. Appl.* **2019**, *8*, 98. [CrossRef] [PubMed]
28. Minatti, G.; Faenzi, M.; Martini, E.; Caminita, F.; De Vita, P.; González-Ovejero, D.; Sabbadini, M.; Maci, S. Modulated Metasurface Antennas for Space: Synthesis, Analysis and Realizations. *IEEE Trans. Antennas Propag.* **2015**, *63*, 1288–1300. [CrossRef]
29. Afzal, M.U.; Esselle, K.P. Steering the beam of medium-to-high gain antennas using near-field phase transformation. *IEEE Trans. Antennas Propag.* **2017**, *65*, 1680–1690. [CrossRef]
30. Baba, A.A.; Hashmi, R.M.; Attygalle, M.; Esselle, K.P.; Borg, D. Ultrawideband Beam Steering at mm-Wave Frequency With Planar Dielectric Phase Transformers. *IEEE Trans. Antennas Propag.* **2022**, *70*, 1719–1728. [CrossRef]
31. Ahmed, F.; Afzal, M.U.; Hayat, T.; Esselle, K.P.; Thalakotuna, D.N. A Near-Field Meta-Steering Antenna System With Fully Metallic Metasurfaces. *IEEE Trans. Antennas Propag.* **2022**, *70*, 10062–10075. [CrossRef]
32. Glybovski, S.B.; Tretyakov, S.A.; Belov, P.A.; Kivshar, Y.S.; Simovski, C.R. Metasurfaces: From microwaves to visible. *Phys. Rep.* **2016**, *634*, 1–72. [CrossRef]
33. Sun, S.; He, Q.; Xiao, S.; Xu, Q.; Li, X.; Zhou, L. Gradient-index meta-surfaces as a bridge linking propagating waves and surface waves. *Nat. Mater.* **2012**, *11*, 426–431. [CrossRef]
34. Vardaxoglou, J.C. *Frequency Selective Surfaces: Analysis and Design*; Research Studies Press: Devon, UK, 1997.
35. Epstein, A.; Eleftheriades, G.V. Huygens' metasurfaces via the equivalence principle: Design and applications. *JOSA B* **2016**, *33*, A31–A50. [CrossRef]
36. Epstein, A.; Eleftheriades, G.V. Arbitrary power-conserving field transformations with passive lossless omega-type bianisotropic metasurfaces. *IEEE Trans. Antennas Propag.* **2016**, *64*, 3880–3895. [CrossRef]
37. Maci, S.; Minatti, G.; Casaletti, M.; Bosiljevac, M. Metasurfing: Addressing waves on impenetrable metasurfaces. *IEEE Antennas Wirel. Propag. Lett.* **2011**, *10*, 1499–1502. [CrossRef]
38. Holloway, C.L.; Love, D.C.; Kuester, E.F.; Gordon, J.A.; Hill, D.A. Use of generalized sheet transition conditions to model guided waves on metasurfaces/metafilms. *IEEE Trans. Antennas Propag.* **2012**, *60*, 5173–5186. [CrossRef]
39. Holloway, C.L.; Kuester, E.F.; Dienstfrey, A. Characterizing metasurfaces/metafilms: The connection between surface susceptibilities and effective material properties. *IEEE Antennas Wirel. Propag. Lett.* **2011**, *10*, 1507–1511. [CrossRef]
40. Holloway, C.L.; Kuester, E. Generalized Sheet Transition Conditions (GSTCs) for a Metascreen: A Subclass of a Metasurface. *IEEE Trans. Antennas Propag.* **2018**, *66*, 2414–2427. [CrossRef]
41. Chen, M.; Kim, M.; Wong, A.M.; Eleftheriades, G.V. Huygens' metasurfaces from microwaves to optics: A review. *Nanophotonics* **2018**, *7*, 1207–1231. [CrossRef]
42. Kuester, E.F.; Mohamed, M.A.; Piket-May, M.; Holloway, C.L. Averaged transition conditions for electromagnetic fields at a metafilm. *IEEE Trans. Antennas Propag.* **2003**, *51*, 2641–2651. [CrossRef]
43. Niemi, T.; Karilainen, A.O.; Tretyakov, S.A. Synthesis of polarization transformers. *IEEE Trans. Antennas Propag.* **2013**, *61*, 3102–3111. [CrossRef]
44. Wong, J.P.; Selvanayagam, M.; Eleftheriades, G.V. Design of unit cells and demonstration of methods for synthesizing Huygens metasurfaces. *Photonics Nanostruct.-Fundam. Appl.* **2014**, *12*, 360–375. [CrossRef]
45. Achouri, K.; Salem, M.A.; Caloz, C. General metasurface synthesis based on susceptibility tensors. *IEEE Trans. Antennas Propag.* **2015**, *63*, 2977–2991. [CrossRef]

46. Bomzon, Z.; Biener, G.; Kleiner, V.; Hasman, E. Space-variant Pancharatnam–Berry phase optical elements with computer-generated subwavelength gratings. *Opt. Lett.* **2002**, *27*, 1141–1143. [CrossRef] [PubMed]

47. Li, Y.; Zhang, J.; Qu, S.; Wang, J.; Pang, Y.; Xu, Z. Ultra-wideband, high-efficiency beam steering based on phase gradient metasurfaces. *J. Electromagn. Waves Appl.* **2015**, *29*, 2163–2170. [CrossRef]

48. Khalid, A.U.R.; Feng, F.; Ullah, N.; Yuan, X.; Somekh, M.G. Exploitation of geometric and propagation phases for spin-dependent rational-multiple complete phase modulation using dielectric metasurfaces. *Photonics Res.* **2022**, *10*, 877–885. [CrossRef]

49. Pfeiffer, C.; Emani, N.K.; Shaltout, A.M.; Boltasseva, A.; Shalaev, V.M.; Grbic, A. Efficient light bending with isotropic metamaterial Huygens' surfaces. *Nano Lett.* **2014**, *14*, 2491–2497. [CrossRef] [PubMed]

50. Gagnon, N.; Petosa, A. Using rotatable planar phase shifting surfaces to steer a high-gain beam. *IEEE Trans. Antennas Propag.* **2013**, *61*, 3086–3092. [CrossRef]

51. Taghvaee, H.; Cabellos-Aparicio, A.; Georgiou, J.; Abadal, S. Error analysis of programmable metasurfaces for beam steering. *IEEE J. Emerg. Sel. Top. Circuits Syst.* **2020**, *10*, 62–74. [CrossRef]

52. Estakhri, N.M.; Alù, A. Wave-front transformation with gradient metasurfaces. *Phys. Rev. X* **2016**, *6*, 041008.

53. Zhu, B.O. Surface impedance synthesis using parallel planar electric metasurfaces. *Prog. Electromagn. Res.* **2017**, *160*, 41–50. [CrossRef]

54. Zhu, B.O.; Xiong, X.Y.; Jiang, L.J. A unified analysis framework for tensor metasurfaces. *J. Opt.* **2018**, *20*, 085102. [CrossRef]

55. Holloway, C.L.; Kuester, E.F.; Gordon, J.A.; O'Hara, J.; Booth, J.; Smith, D.R. An overview of the theory and applications of metasurfaces: The two-dimensional equivalents of metamaterials. *IEEE Antennas Propag. Mag.* **2012**, *54*, 10–35. [CrossRef]

56. Pfeiffer, C.; Grbic, A. Millimeter-wave transmitarrays for wavefront and polarization control. *IEEE Trans. Microw. Theory Tech.* **2013**, *61*, 4407–4417. [CrossRef]

57. Pfeiffer, C.; Grbic, A. Bianisotropic metasurfaces for optimal polarization control: Analysis and synthesis. *Phys. Rev. Appl.* **2014**, *2*, 044011. [CrossRef]

58. Epstein, A.; Eleftheriades, G.V. Passive lossless Huygens metasurfaces for conversion of arbitrary source field to directive radiation. *IEEE Trans. Antennas Propag.* **2014**, *62*, 5680–5695. [CrossRef]

59. Bodehou, M.; Craeye, C.; Huynen, I. Electric Field Integral Equation-Based Synthesis of Elliptical-Domain Metasurface Antennas. *IEEE Trans. Antennas Propag.* **2018**, *67*, 1270–1274. [CrossRef]

60. Zhu, B.O. Metasurface Synthesis With Arbitrary Incident Angles Using Planar Electric Impedance Surfaces. *IEEE J. Multiscale Multiphys. Comput. Tech.* **2019**, *4*, 51–56. [CrossRef]

61. Egorov, G.A.; Eleftheriades, G.V. Theory and Simulation of Metasurface Lenses for Extending the Angular Scan Range of Phased Arrays. *arXiv* **2020**, arXiv:2001.04556.

62. Selvanayagam, M.; Eleftheriades, G.V. Polarization control using tensor Huygens surfaces. *IEEE Trans. Antennas Propag.* **2014**, *62*, 6155–6168. [CrossRef]

63. Salem, M.A.; Achouri, K.; Caloz, C. Metasurface synthesis for time-harmonic waves: Exact spectral and spatial methods. *Prog. Electromagn. Res.* **2014**, *149*, 205–216. [CrossRef]

64. Salem, M.A.; Caloz, C. Manipulating light at distance by a metasurface using momentum transformation. *Opt. Express* **2014**, *22*, 14530–14543. [CrossRef]

65. Smy, T.J.; Rahmeier, J.G.N.; Dugan, J.; Gupta, S. Part II-Spatially Dispersive Metasurfaces: IE-GSTC-SD Field Solver with Extended GSTCs. *IEEE Trans. Antennas Propag.* **2022**. [CrossRef]

66. Lavigne, G.; Achouri, K.; Asadchy, V.S.; Tretyakov, S.A.; Caloz, C. Susceptibility derivation and experimental demonstration of refracting metasurfaces without spurious diffraction. *IEEE Trans. Antennas Propag.* **2018**, *66*, 1321–1330. [CrossRef]

67. Jia, X.; Vahabzadeh, Y.; Caloz, C.; Yang, F. Synthesis of spherical metasurfaces based on susceptibility tensor GSTCs. *IEEE Trans. Antennas Propag.* **2019**, *67*, 2542–2554. [CrossRef]

68. Momeni, A.; Rajabalipanah, H.; Abdolali, A.; Achouri, K. Generalized optical signal processing based on multioperator metasurfaces synthesized by susceptibility tensors. *Phys. Rev. Appl.* **2019**, *11*, 064042. [CrossRef]

69. Dugan, J.; Smy, T.J.; Gupta, S. Accelerated ie-gstc solver for large-scale metasurface field scattering problems using fast multipole method (fmm). *IEEE Trans. Antennas Propag.* **2022**, *70*, 9524–9533. [CrossRef]

70. Asadchy, V.S.; Albooyeh, M.; Tcvetkova, S.N.; Díaz-Rubio, A.; Ra'di, Y.; Tretyakov, S. Perfect control of reflection and refraction using spatially dispersive metasurfaces. *Phys. Rev. B* **2016**, *94*, 075142. [CrossRef]

71. Epstein, A.; Eleftheriades, G.V. Arbitrary antenna arrays without feed networks based on cavity-excited omega-bianisotropic metasurfaces. *IEEE Trans. Antennas Propag.* **2017**, *65*, 1749–1756. [CrossRef]

72. Singh, K.; Afzal, M.U.; Kovaleva, M.; Esselle, K.P. Controlling the Most Significant Grating Lobes in Two-Dimensional Beam-Steering Systems with Phase-Gradient Metasurfaces. *IEEE Trans. Antennas Propag.* **2019**, *68*, 1389–1401. [CrossRef]

73. Ra'di, Y.; Sounas, D.L.; Alù, A. Metagratings: Beyond the limits of graded metasurfaces for wave front control. *Phys. Rev. Lett.* **2017**, *119*, 067404. [CrossRef]

74. Díaz-Rubio, A.; Asadchy, V.S.; Elsakka, A.; Tretyakov, S.A. From the generalized reflection law to the realization of perfect anomalous reflectors. *Sci. Adv.* **2017**, *3*, e1602714. [CrossRef]

75. Wong, A.M.; Eleftheriades, G.V. Perfect anomalous reflection with a bipartite Huygens' metasurface. *Phys. Rev. X* **2018**, *8*, 011036. [CrossRef]

76. Casolaro, A.; Toscano, A.; Alù, A.; Bilotti, F. Dynamic Beam Steering with Reconfigurable Metagratings. *IEEE Trans. Antennas Propag.* **2019**, *68*, 1542–1552. [CrossRef]

77. Popov, V.; Yakovleva, M.; Boust, F.; Pelouard, J.L.; Pardo, F.; Burokur, S.N. Designing metagratings via local periodic approximation: From microwaves to infrared. *Phys. Rev. Appl.* **2019**, *11*, 044054. [CrossRef]

78. Popov, V.; Boust, F.; Burokur, S.N. Beamforming with metagratings at microwave frequencies: Design procedure and experimental demonstration. *IEEE Trans. Antennas Propag.* **2019**, *68*, 1533–1541. [CrossRef]

79. Popov, V.; Boust, F.; Burokur, S.N. Controlling diffraction patterns with metagratings. *Phys. Rev. Appl.* **2018**, *10*, 011002. [CrossRef]

80. Li, L.; Wang, J.; Qu, S. A broadband polarization rotation phase gradient metasurface designed by all-dielectric high-permittivity ceramic blocks. In Proceedings of the 2021 IEEE MTT-S International Microwave Workshop Series on Advanced Materials and Processes for RF and THz Applications (IMWS-AMP), Chongqing, China, 15–17 November 2021; pp. 154–156.

81. Hayat, T.; Afzal, M.U.; Ahmed, F.; Zhang, S.; Esselle, K.P.; Vardaxoglou, J. The Use of a Pair of 3D-Printed Near Field Superstructures to Steer an Antenna Beam in Elevation and Azimuth. *IEEE Access* **2021**, *9*, 153995–154010. [CrossRef]

82. Nooshnab, S.; Golmohammadi, S.; Baghban, H. Enhanced Nonlinear Harmonic Signal Emission by an Electromagnetically Induced Transparency Resonant All-Dielectric Metasurface. *IEEE Trans. Nanotechnol.* **2022**, *21*, 514–521. [CrossRef]

83. Faenzi, M.; Minatti, G.; Gonzalez-Ovejero, D.; Caminita, F.; Martini, E.; Della Giovampaola, C.; Maci, S. lMetasurface antennas: New models, applications and realizations. *Sci. Rep.* **2019**, *9*, 10178. [CrossRef]

84. Nizer Rahmeier, J.G.; Smy, T.J.; Dugan, J.; Gupta, S. Part I-Spatially Dispersive Metasurfaces: Zero Thickness Surface Susceptibilities & Extended GSTCs. *IEEE Trans. Antennas Propag.* **2022**. [CrossRef]

85. Singh, K.; Afzal, M.U.; Esselle, K.P. Designing Efficient Phase-Gradient Metasurfaces for Near-Field Meta-Steering Systems. *IEEE Access* **2021**, *9*, 109080–109093. [CrossRef]

86. Singh, K.; Afzal, M.U.; Esselle, K.P. Accurate optimization technique for phase-gradient metasurfaces used in compact near-field meta-steering systems. *Sci. Rep.* **2022**, *12*, 4118. [CrossRef] [PubMed]

87. Ahmed, F.; Afzal, M.U.; Hayat, T.; Esselle, K.P.; Thalakotuna, D.N. A Dielectric Free Near Field Phase Transforming Structure for Wideband Gain Enhancement of Antennas. *Sci. Rep.* **2021**, *11*, 14613. [CrossRef] [PubMed]

88. Ahmed, F.; Afzal, M.U.; Hayat, T.; Esselle, K.P.; Thalakotuna, D.N. Self-Sustained Rigid Fully Metallic Metasurfaces to Enhance Gain of Shortened Horn Antennas. *IEEE Access* **2022**, *10*, 79644–79654. [CrossRef]

89. Ahmed, F.; Hayat, T.; Afzal, M.U.; Lalbakhsh, A.; Esselle, K.P. Dielectric-Free Cells for Low-Cost Near-Field Phase Shifting Metasurfaces. In Proceedings of the 2020 IEEE International Symposium on Antennas and Propagation and North American Radio Science Meeting, Montreal, QC, Canada, 5–10 July 2020; pp. 741–742.

90. Ahmed, F.; Afzal, M.U.; Hayat, T.; Thalakotuna, D.; Esselle, K. Near-Field Phase Transforming Structures for High-Performance Antenna Systems. In Proceedings of the 2022 IEEE International Symposium on Antennas and Propagation and USNC-URSI Radio Science Meeting (AP-S/URSI), Denver, CO, USA, 10–15 July 2022; pp. 1640–1641.

91. Tasolamprou, A.C.; Skoulas, E.; Perrakis, G.; Vlahou, M.; Viskadourakis, Z.; Economou, E.N.; Kafesaki, M.; Kenanakis, G.; Stratakis, E. Highly ordered laser imprinted plasmonic metasurfaces for polarization sensitive perfect absorption. *Sci. Rep.* **2022**, *12*, 19769. [CrossRef]

92. Ataloglou, V.G.; Chen, M.; Kim, M.; Eleftheriades, G.V. Microwave Huygens' metasurfaces: Fundamentals and applications. *IEEE J. Microwaves* **2021**, *1*, 374–388. [CrossRef]

93. Barbarić, D.; Šipuš, Z. Designing metasurfaces with canonical unit cells. *Crystals* **2020**, *10*, 938. [CrossRef]

94. Singh, K.; Afzal, M.U.; Esselle, K.P.; Kovaleva, M. Towards Decreasing Side Lobes Produced by Near-Field Phase Gradient Metasurfaces. In Proceedings of the 2019 IEEE International Symposium on Antennas and Propagation and USNC-URSI Radio Science Meeting, Atlanta, GA, USA, 7–12 July 2019; pp. 1207–1208.

95. Su, J.; Lu, Y.; Liu, J.; Yang, Y.; Li, Z.; Song, J. A novel checkerboard metasurface based on optimized multielement phase cancellation for superwideband RCS reduction. *IEEE Trans. Antennas Propag.* **2018**, *66*, 7091–7099. [CrossRef]

96. Elsawy, M.M.; Lanteri, S.; Duvigneau, R.; Brière, G.; Mohamed, M.S.; Genevet, P. Global optimization of metasurface designs using statistical learning methods. *Sci. Rep.* **2019**, *9*, 17918. [CrossRef]

97. Singh, K.; Afzal, M.U.; Esselle, K.P. An Overview On the Optimization of Beam-Steering Metasurfaces. In Proceedings of the 2021 XXXIVth General Assembly and Scientific Symposium of the International Union of Radio Science (URSI GASS), Rome, Italy, 28 August–4 September 2021; pp. 01–04.

98. Monti, A.; Alù, A.; Toscano, A.; Bilotti, F. Design of high-Q passband filters implemented through multipolar all-dielectric metasurfaces. *IEEE Trans. Antennas Propag.* **2020**, *69*, 5142–5147. [CrossRef]

99. Epstein, A.; Eleftheriades, G.V. Synthesis of passive lossless metasurfaces using auxiliary fields for reflectionless beam splitting and perfect reflection. *Phys. Rev. Lett.* **2016**, *117*, 256103. [CrossRef]

100. Ghosh, S.; Lim, S. Fluidically Switchable Metasurface for Wide Spectrum Absorption. *Sci. Rep.* **2018**, *8*, 10169. [CrossRef]

101. Vellucci, S.; Monti, A.; Barbuto, M.; Toscano, A.; Bilotti, F. Satellite applications of electromagnetic cloaking. *IEEE Trans. Antennas Propag.* **2017**, *65*, 4931–4934. [CrossRef]

102. Achouri, K.; Caloz, C. Space-wave routing via surface waves using a metasurface system. *Sci. Rep.* **2018**, *8*, 7549. [CrossRef]

103. Li, L.; Zhang, X.; Song, C.; Zhang, W.; Jia, T.; Huang, Y. Compact dual-band, wide-angle, polarization-angle-independent rectifying metasurface for ambient energy harvesting and wireless power transfer. *IEEE Trans. Microw. Theory Tech.* **2020**, *69*, 1518–1528. [CrossRef]

104. Dong, F.; Chu, W. Multichannel-Independent Information Encoding with Optical Metasurfaces. *Adv. Mater.* **2019**, *31*, 1804921. [CrossRef] [PubMed]
105. Samantaray, D.; Bhattacharyya, S. A gain-enhanced slotted patch antenna using metasurface as superstrate configuration. *IEEE Trans. Antennas Propag.* **2020**, *68*, 6548–6556. [CrossRef]
106. Usha, P.; Krishnan, C. Epsilon Near Zero Metasurface for Ultrawideband Antenna Gain Enhancement and Radar Cross Section Reduction. *AEU-Int. J. Electron. Commun.* **2020**, *19*, 153167. [CrossRef]
107. Katare, K.K.; Chandravanshi, S.; Biswas, A.; Akhtar, M.J. Realization of split beam antenna using transmission-type coding metasurface and planar lens. *IEEE Trans. Antennas Propag.* **2019**, *67*, 2074–2084. [CrossRef]
108. Bodehou, M.; Martini, E.; Maci, S.; Huynen, I.; Craeye, C. Multibeam and beam scanning with modulated metasurfaces. *IEEE Trans. Antennas Propag.* **2019**, *68*, 1273–1281. [CrossRef]
109. Li, H.; Wang, G.; Ji, W.; Cai, T.; Gao, X.; Hou, H. Focusing MSs for high-gain antenna applications. In *Metamaterials Metasurfaces*; IntechOpen: Rijeka, Croatia, 2018.
110. Fan, J.; Cheng, Y. Broadband high-efficiency cross-polarization conversion and multi-functional wavefront manipulation based on chiral structure metasurface for terahertz wave. *J. Phys. D Appl. Phys.* **2019**, *53*, 025109. [CrossRef]
111. Soares, I.; Resende, U. Radially Periodic Metasurface Lenses for Magnetic Field Collimation in Resonant Wireless Power Transfer Applications. *J. Microw. Optoelectron. Electromagn. Appl.* **2022**, *21*, 48–60. [CrossRef]
112. Zhang, S. Intelligent metasurfaces: Digitalized, programmable, and intelligent platforms. *Light Sci. Appl.* **2022**, *11*, 242. [CrossRef] [PubMed]
113. Sleasman, T.; Boyarsky, M.; Pulido-Mancera, L.; Fromenteze, T.; Imani, M.F.; Reynolds, M.S.; Smith, D.R. Experimental synthetic aperture radar with dynamic metasurfaces. *IEEE Trans. Antennas Propag.* **2017**, *65*, 6864–6877. *IEEE Trans. Antennas Propag.* **2017**, *65*, 6864–6877. [CrossRef]
114. Lan, G.; Imani, M.F.; del Hougne, P.; Hu, W.; Smith, D.R.; Gorlatova, M. Wireless Sensing using Dynamic Metasurface Antennas: Challenges and Opportunities. *IEEE Commun. Mag.* **2020**, *58*, 66–71. [CrossRef]
115. Islam, M.T.; Samsuzzaman, M.; Kibria, S.; Misran, N.; Islam, M.T. Metasurface Loaded High Gain Antenna based Microwave Imaging using Iteratively Corrected Delay Multiply and Sum Algorithm. *Sci. Rep.* **2019**, *9*, 17317. [CrossRef] [PubMed]
116. Kou, N.; Liu, H.; Li, L. A transplantable frequency selective metasurface for high-order harmonic suppression. *Appl. Sci.* **2017**, *7*, 1240. [CrossRef]
117. Bernard, L.; Martinis, M.; Collardey, S.; Mahdjoubi, K.; Sauleau, R. Metasurface antennas embedded in small circular cavities for telemetry applications. *Appl. Sci.* **2019**, *9*, 2496. [CrossRef]
118. Wang, J.; Li, Y.; Jiang, Z.H.; Shi, T.; Tang, M.C.; Zhou, Z.; Chen, Z.N.; Qiu, C.W. Metantenna: When Metasurface Meets Antenna Again. *IEEE Trans. Antennas Propag.* **2020**, *68*, 1332–1347. [CrossRef]
119. Liu, R.; Wang, X.; Nie, D.; Wang, L.; Cui, W.; Wang, M.; Zheng, H.; Li, E. Metasurface: Enhancing gain of antenna and energy harvesting system design. *Int. J. Microw. Comput.-Aided Eng.* **2020**, *30*, e22053. [CrossRef]
120. Suriyakala, C.D.; Eldhose, A. Meta surface enabled wearable antenna for medical implant applications. In Proceedings of the 2017 International Conference on Circuit ,Power and Computing Technologies (ICCPCT), Kollam, India, 20–21 April 2017; pp. 1–6.
121. Marks, D.L.; Yurduseven, O.; Smith, D.R. Cavity-backed metasurface antennas and their application to frequency diversity imaging. *JOSA A* **2017**, *34*, 472–480. [CrossRef]
122. Liu, S.; Yang, D.; Chen, Y.; Zhang, X.; Xiang, Y. Compatible Integration of Circularly Polarized Omnidirectional Metasurface Antenna With Solar Cells. *IEEE Trans. Antennas Propag.* **2019**, *68*, 4155–4160. [CrossRef]
123. Ta, S.X.; Lee, J.J.; Park, I. Solar-Cell Metasurface-Integrated Circularly Polarized Antenna With 100 *IEEE Antennas Wirel. Propag. Lett.* **2017**, *16*, 2675–2678.
124. Ni, X.; Emani, N.K.; Kildishev, A.V.; Boltasseva, A.; Shalaev, V.M. Broadband light bending with plasmonic nanoantennas. *Science* **2012**, *335*, 427–427. [CrossRef] [PubMed]
125. Zhang, X.; Tian, Z.; Yue, W.; Gu, J.; Zhang, S.; Han, J.; Zhang, W. Broadband terahertz wave deflection based on C-shape complex metamaterials with phase discontinuities. *Adv. Mater.* **2013**, *25*, 4567–4572. [CrossRef] [PubMed]
126. Cui, T.J.; Qi, M.Q.; Wan, X.; Zhao, J.; Cheng, Q. Coding metamaterials, digital metamaterials and programmable metamaterials. *Light Sci. Appl.* **2014**, *3*, e218. [CrossRef]
127. Liu, S.; Cui, T.J.; Xu, Q.; Bao, D.; Du, L.; Wan, X.; Tang, W.X.; Ouyang, C.; Zhou, X.Y.; Yuan, H.; et al. Anisotropic coding metamaterials and their powerful manipulation of differently polarized terahertz waves. *Light Sci. Appl.* **2016**, *5*, e16076. [CrossRef] [PubMed]
128. Pancharatnam, S. Generalized theory of interference and its applications. *Proc. Indian Acad. Sci.-Sect. A* **1956**, *44*, 398–417. [CrossRef]
129. Berry, M.V. Quantal phase factors accompanying adiabatic changes. *Proc. R. Soc. Lond. A Math. Phys. Sci.* **1984**, *392*, 45–57.
130. Huang, L.; Chen, X.; Muhlenbernd, H.; Li, G.; Bai, B.; Tan, Q.; Jin, G.; Zentgraf, T.; Zhang, S. Dispersionless phase discontinuities for controlling light propagation. *Nano Lett.* **2012**, *12*, 5750–5755. [CrossRef]
131. Arbabi, A.; Faraon, A. Fundamental limits of ultrathin metasurfaces. *Sci. Rep.* **2017**, *7*, 43722. [CrossRef] [PubMed]
132. Ding, X.; Monticone, F.; Zhang, K.; Zhang, L.; Gao, D.; Burokur, S.N.; de Lustrac, A.; Wu, Q.; Qiu, C.W.; Alu, A. Ultrathin Pancharatnam–Berry metasurface with maximal cross-polarization efficiency. *Adv. Mater.* **2015**, *27*, 1195–1200. [CrossRef] [PubMed]

133. Zheng, G.; Muhlenbernd, H.; Kenney, M.; Li, G.; Zentgraf, T.; Zhang, S. Metasurface holograms reaching 80% efficiency. *Nat. Nanotechnol.* **2015**, *10*, 308–312. [CrossRef] [PubMed]

134. Luo, W.; Sun, S.; Xu, H.X.; He, Q.; Zhou, L. Transmissive ultrathin Pancharatnam-Berry metasurfaces with nearly 100% efficiency. *Phys. Rev. Appl.* **2017**, *7*, 044033. [CrossRef]

135. Qu, M.; Li, S.; Deng, L.; Ma, X. Focusing Metasurface with arbitrary Focal Point Based on Pancharatnam-Berry Phase Principle. In Proceedings of the 2019 IEEE International Symposium on Antennas and Propagation and USNC-URSI Radio Science Meeting, Atlanta, GA, USA, 7–12 July 2019; pp. 445–446.

136. Yang, P.; Dang, R.; Li, L. Dual-Linear-to-Circular Polarization Converter Based Polarization-Twisting Metasurface Antenna for Generating Dual Band Dual Circularly Polarized Radiation in Ku-band. *IEEE Trans. Antennas Propag.* **2022**, *70*, 9877–9881. [CrossRef]

137. Li, S.; Dong, S.; Yi, S.; Pan, W.; Chen, Y.; Guan, F.; Guo, H.; Wang, Z.; He, Q.; Zhou, L.; et al. Broadband and high-efficiency spin-polarized wave engineering with PB metasurfaces. *Opt. Express* **2020**, *28*, 15601–15610. [CrossRef] [PubMed]

138. Ta, S.X.; Park, I.; Ziolkowski, R.W. Circularly Polarized Crossed Dipole on an HIS for 2.4/5.2/5.8-GHz WLAN Applications. *IEEE Antennas Wirel. Propag. Lett.* **2013**, *12*, 1464–1467. [CrossRef]

139. Tran, H.H.; Park, I. A Dual-Wideband Circularly Polarized Antenna Using an Artificial Magnetic Conductor. *IEEE Antennas Wirel. Propag. Lett.* **2016**, *15*, 950–953. [CrossRef]

140. Chen, M.L.; Jiang, L.J.; Sha, W.E. Artificial perfect electric conductor-perfect magnetic conductor anisotropic metasurface for generating orbital angular momentum of microwave with nearly perfect conversion efficiency. *J. Appl. Phys.* **2016**, *119*, 064506. [CrossRef]

141. Zhang, Y.; Wang, Z.; Ren, Y.; Pan, C.; Zhang, J.; Jia, L.; Zhu, X. A Novel Metasurface Lens Design for Synthesizing Plane Waves in Millimeter-Wave Bands. *Electronics* **2022**, *11*, 1403. [CrossRef]

142. Singh, K.; Afzal, M.U.; Lalbakhsh, A.; Esselle, K.P. Reflecting Phase-Gradient Metasurface for Radar Cross Section Reduction. In Proceedings of the 2021 IEEE Asia-Pacific Microwave Conference (APMC), Brisbane, Australia, 28 November–1 December 2021; pp. 344–346.

143. Zhong, Y.C.; Cheng, Y.J. Generating and Steering Quasi-Nondiffractive Beam by Near-Field Planar Risley Prisms. *IEEE Trans. Antennas Propag.* **2020**, *68*, 7767–7776. [CrossRef]

144. Smith, D.R.; Yurduseven, O.; Mancera, L.P.; Bowen, P.; Kundtz, N.B. Analysis of a waveguide-fed metasurface antenna. *Phys. Rev. Appl.* **2017**, *8*, 054048. [CrossRef]

145. Li, H.; Wang, G.; Gao, X.; Liang, J.; Hou, H. A Novel Metasurface for Dual-Mode and Dual-Band Flat High-Gain Antenna Application. *IEEE Trans. Antennas Propag.* **2018**, *66*, 3706–3711. [CrossRef]

146. Li, H.; Wang, G.; Xu, H.X.; Cai, T.; Liang, J. X-band phase-gradient metasurface for high-gain lens antenna application. *IEEE Trans. Antennas Propag.* **2015**, *63*, 5144–5149. [CrossRef]

147. Pfeiffer, C.; Grbic, A. Planar lens antennas of subwavelength thickness: Collimating leaky-waves with metasurfaces. *IEEE Trans. Antennas Propag.* **2015**, *63*, 3248–3253. [CrossRef]

148. Hou, H.; Li, H.; Wang, G.; Cai, T.; Gao, X.; Guo, W. High Performance Metasurface Antennas. In *Dielectric and Other Metasurfaces—From Fundamentals to Applications*; IntechOpen: London, UK, 2019.